







Updated Orbital Decay Rate of WASP-12 with New Data from TESS and Ground-based Observations

Ahmet Cem Kutluay¹  , Özgür Baştürk² , Selçuk Yalçinkaya² , Tenay Saguner¹ ,
Sinan Kaan Yerli¹ 

¹ Orta Doğu Teknik Üniversitesi, Physics Department, 06800, Ankara, Türkiye

² Ankara University, Faculty of Science, Astronomy and Space Sciences Department, 06100, Ankara, Türkiye

Accepted: September 6, 2023. Revised: August 21, 2023. Received: May 31, 2023.

Abstract

We investigate the orbital decay behavior of the well-studied hot Jupiter WASP-12 b orbiting its late-F host star on a 1.09-day orbit by analyzing its transit timings. Thanks to precise photometric data covering nearly 15 years of observations from the space and the ground since the discovery of the planet, including a transit light curve of our own, it became possible to study this behaviour in its details. This work updates the orbital period to a new value of $P = 1.0914202527 \pm 0.000000039$ days and agrees with the previous finding that the planetary orbit has been shrinking with an updated rate of $-31.03 \pm 0.94 \text{ ms yr}^{-1}$. This corresponds to an orbital decay timescale of $\tau = P/|\dot{P}| = 3.04 \pm 0.09 \text{ Myr}$ that we attribute to the strong tidal interactions between the host-star and the planet. We also update the reduced stellar tidal quality factor as $Q'_* = (1.72 \pm 0.39) \times 10^5$, which corresponds to the lower bound of the previously reported values of the parameter.

Özet

Bu çalışmada, geç F tayf türünden bir barınak yıldızın etrafında 1.09 günlük bir yörünge döneminde dolanan, çok çalışılmış WASP-12 b sıcak Jupiter türü gezegenin geçiş zamanlarını inceleyerek yörünge küçülme davranışı gösterip göstermediğini araştırdık. Keşfinden beri, neredeyse 15 yılı kapsayan, hem uzaydan hem yerden elde edilen fotometrik veri, hem de bizim kendimize ait bir gözlemimiz sayesinde, bahsi geçen yörünge küçülmesini detaylarıyla incelemek mümkün oldu. Bu çalışma gezegenin yörünge dönemini $P = 1.0914202527 \pm 0.000000039$ gün olarak güncellemesinin yanı sıra gezegenin yörüngesinin sabit bir oran ile küçüldüğünü doğrulamakta ve bu oran $-31.03 \pm 0.94 \text{ ms yıl}^{-1}$ olarak verilmektedir. Bu bulgunun işaret ettiği yörünge küçülmesi zaman ölçeği $\tau = P/|\dot{P}| = 3.04 \pm 0.09$ Milyon yıl olarak bulunmuştur. Yörünge dönemindeki bu kısımla gezegen ve barınak yıldızı arasındaki tedirginlik etkilerine atfedilmiştir. Ek olarak, bu çalışmada yıldızın tedirginlik etkileşimleri sonucu açığa çıkan enerjiyi alma kapasitesini ifade eden tedirginlik kalite faktörü $Q'_* = (1.72 \pm 0.39) \times 10^5$ olarak bulunmuştur. Bu değer, daha önceki çalışmalarda rapor edilmiş değer aralığının alt sınırındadır.

Key words: orbital decay – methods: data analysis – techniques: photometric – stars: individual: WASP-12 – planetary systems

1 Introduction

WASP-12 b is an ultra-hot Jupiter-type planet with a $1.5 M_{\text{Jup}}$ mass and an inflated radius of $1.9 R_{\text{Jup}}$ (Collins et al. 2017b), orbiting a late F-type star having a surface temperature of 6150K on a short-period orbit of 1.09 days (Stassun et al. 2019). It was discovered by Hebb et al. (2009), has attracted a great deal of attention in the exoplanet community since its discovery, and has been the subject of numerous studies due to the anomalies in the long-term transit data (Maciejewski et al. 2013, 2016) and the transits themselves (Llama et al. 2013), enabling us to investigate the evolutionary history of the system. We provide fundamental parameters of the system and their references which we made use of in our calculations in Table 1.

In theory, while the stellar evolution is determined by the thermonuclear reactions at the core, the rate of which is decided by stellar mass, the stellar rotation rate slows down with the evolution of magnetic activity in stars with convective envelopes

(Skumanich 1972), explained within the general framework of the magnetic dynamo hypothesis (Babcock 1961). On the other hand, orbital evolution of planets depends on their interactions with other bodies gravitationally bound to the system and the protoplanetary disk structure soon after they form. Although there are in-situ formation mechanisms favorable only for a few special cases (Bailey & Batygin 2018), hot-Jupiters are theorized to be forming at larger distances beyond the snow line of at least water and then migrate inwards through interactions with the protoplanetary disk (disk interaction migration) (Chambers 2007; D'Angelo et al. 2010) or with a massive body outside, through Kozai-Lidov mechanism (high eccentricity migration) (Knutson et al. 2014). Then they end up at the close vicinity of their host stars where they are observed now and are subject to strong tidal interactions with them. During the evolution of the system, the spin and orbital period also evolve over very long timescales, which is complicated by the strong tidal interactions between the planet and the host-star (Ogilvie 2014) when they get even closer due to inward migration. For a typical hot Jupiter, tidal friction is expected to align the axis of the stellar spin with that of the orbit and

* ackutluay@gmail.com

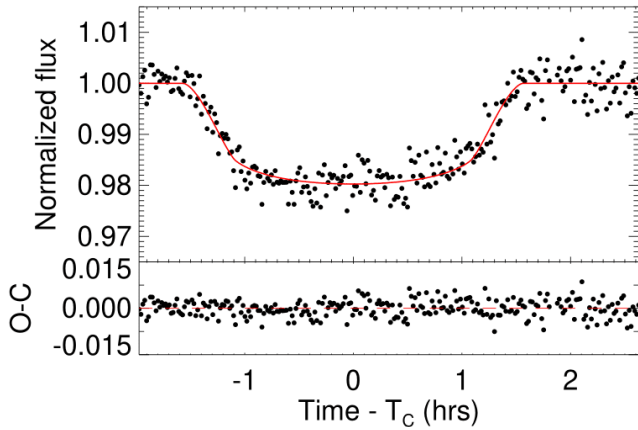


Figure 1. Normalized light curve of WASP-12 obtained through the observation made on 3 Nov 2022 at Kreiken Observatory. The residuals are shown in the bottom plot.

causes the orbit to decay within similar timescales (Barker & Ogilvie 2009).

First, Maciejewski et al. (2016) reported that the orbital period of WASP-12 b was decreasing causing long-term transit timing variations (hereafter TTVs), but the reason for this change was unclear and could have been due to different factors, such as orbital decay, apsidal precession, light-time or Rømer effect due to another body in the system (Bechter et al. 2014). Later, follow-up observations by Patra et al. (2017); Maciejewski et al. (2018); Yee et al. (2020); Turner et al. (2021); Wong et al. (2022); Hagey et al. (2022) confirmed the change, and quadratic models that well-fit the TTV data suggested that orbital decay might be the cause of the observed secular variation. Most recently, Wong et al. (2022) used new observations coming from the Transiting Exoplanet Survey Satellite (TESS; Ricker et al. 2015) recorded during the sectors 43, 44 and 45 and provided compelling evidence that the secular change is continuing which strengthens the potential of an orbital decay.

We have been following WASP-12 b's period change, observed the system once with the 80 cm telescope located at Ankara University Kreiken Observatory (AUKR) (named as T80 Prof.Dr. Berahitdin Albayrak Telescope), and obtained the latest TESS observations to perform its long-term TTV analysis as a follow-up study to check if the decrease in the orbital period still continues and update the TTV parameters as a result (Winn 2019). Our results confirm the persistence of the decrease in the orbital period, supporting the orbital decay explanation due to strong tidal interactions with the host star. We present the observations and data reduction in Section 2, and our data analysis method in Section 3, then we provide our results and their discussion in Section 4, and finally we summarize our work within Section 5.

2 Observations and data reduction

2.1 Observations

We observed a transit of WASP-12 b with the T80 telescope on 3 Nov 2022. The Ritchey–Chrétien design telescope has an 80 cm diameter primary mirror with $f/7$ focal ratio which is equivalent to $37''/\text{mm}$ plate scale, and an $11'.84 \times 11'.84$ field of view (FoV) is achieved on a 1024×1024 back-illuminated CCD

Table 1. Fundamental system parameters for WASP-12 used in this study. 1: Chakrabarty & Sengupta (2019), 2: Gaia Collaboration et al. (2016, 2022), 3: Collins et al. (2017b), 4: Stassun et al. (2019), 5: This work

Parameter	Value	Source
Stellar Parameters		
M_* (M_\odot)	1.170 ± 0.110	1
R_* (R_\odot)	1.657 ± 0.046	1
$\log g$	$3.95^{+0.03}_{-0.09}$	2
[Fe/H] (dex)	$0.33^{+0.014}_{-0.17}$	3
T_{eff} (K)	6154 ± 105	4
Planetary Parameters		
M_p (M_{jup})	1.465 ± 0.079	1
R_p (R_{jup})	1.937 ± 0.056	1
a (au)	0.02320 ± 0.00064	1
P_{orb} (days)	$1.091420253 \pm (3.9 \times 10^{-8})$	5
T_c (BJD _{TDB})	$2459887.49011 \pm 0.00044$	5

having a pixel size of $13 \mu\text{m}$. The observations were performed using an SDSS- r filter slightly defocused with a 60 s exposure time. Therefore, we were able to obtain 262 data points during the entire observing run. We provide the light curve of this observation in Fig. 1.

2.2 Data Reduction

2.2.1 T80 Observations

The CCD images were corrected for the instrumental effects (flat-bias-dark corrections) with AstrolmageJ (hereafter AIJ, Collins et al. 2017a) in the standard manner by using the calibration images obtained during the same observing run. We made use of a group of comparison stars for the ensemble and differential photometry (Honeycutt 1992); and thoroughly examined the possibility of each star exhibiting variability. Afterward, we obtained the light curves by comparing each star to the most suitable set of comparison stars based on their proximity, magnitude, color, and variability. To prevent inaccuracies in the positions of the flux centers caused by defocusing on CCD images, we opted to locate the centers of the apertures through visual means instead of relying on centroid methods which could result in incorrect positions for the 'ring-like' shapes of the stellar signal. Lastly, we removed the influence of the airmass effect on the light curves by employing a linear trend in the out-of-transit data.

2.2.2 Light Curves from the Literature and Open Databases

Additionally, the light-curves of transits were obtained through different resources: literature, open databases such as Exoplanet Transit Database (ETD), ExoClock and AXA Observers. We analyzed the light curves collected from these databases using AIJ. Observers uploading their light curves to ETD assign an integer number (ranging from 0 to 5) to indicate the quality of their data (Poddany et al. 2010). In order to construct a better TTV diagram, we selected only the light curves with a data quality factor better than 2 (≤ 2) not to be affected by the gaps or excessive noise in the data which hamper the measurements of the mid-transit times. Observation timings were corrected to the BJD_{TDB} reference based on the location of the observing facility if they had not been already corrected.

2.2.3 Airmass Detrending and Normalization

The airmass values were calculated using a Python script based on the following equation (Hiltner 1962):

$$X = \sec z - 0.0018167(\sec z - 1) - 0.002875(\sec z - 1)^2 - 0.0008083(\sec z - 1)^3 \quad (1)$$

The light curves were then airmass-detrended and normalized to out-of-transit flux by a simple division to the mean level of out-of-transit fluxes.

2.2.4 TESS Observations

TESS observations during the sectors 20, 43, 44, and 45 between 23 Dec 2019 and 2 Dec 2021 are in public use through the Mikulski Archive for Space Telescopes (MAST). Short-cadence mode, which has 2-minute integration times, was employed during all these sectors for WASP-12. We preferred using the fluxes corrected for instrumental effects based on Co-trending Basis Vectors (CBVs) and stellar variability, hence, we made use of the Data Validation Timeseries (DVT) measurements of the fluxes listed in the LC_DETRENDED column of the relevant DVT-files provided by the TESS Science Processing Operations Center (SPOC) pipeline (Jenkins et al. 2016). To further improve the accuracy and precision, we eliminated any apparent outliers caused by instrumental artifacts and divided the complete data set into smaller segments centered on individual transits. Hence, we obtained 20 precise transit light curves from Sector 20, 19 from Sector 43, 19 from Sector 44, and 21 from Sector 45, adding up to 79 2-minute light curves in total which we provide all in Fig. A1 in the Appendix A.

3 Data Analysis

We obtained, reduced and prepared 62 light curves from ETD (Table A1), 74 light curves from previous studies (Table A2), 79 light curves from TESS observations (Table A3) and a light curve from T80 telescope for the TTV analysis of WASP-12b, forming nearly 15 years of a baseline of photometric observations of planetary transits.

3.1 Light-curve modelling

In order to obtain the mid-transit times and their corresponding errors, we modeled our light curves with the first version of the well-established modeling suite EXOFAST (Eastman et al. 2013), which is also available with a web-based service through NASA Exoplanet Archive. While utilizing the prior and prior width inputs, the measurements from Chakrabarty & Sengupta (2019) were employed. We provided the center and width of the Gaussian priors for our parameters such as R_p/R_* , i , a/R_* , T_{eff} , $[\text{Fe}/\text{H}]$ and the orbital period P_{orb} as given by Chakrabarty & Sengupta (2019). We selected the passband of observations according to the filter used during the observations. While standard Johnson filters were selected for all passbands with close wavelength transmission functions (Johnson-Cousins, Bessel), CoRoT passband was selected for clear observations as an input to determine the priors for the coefficients of the quadratic limb darkening law. This version of the software (EXOFAST-v1) fits the transit light curve with the AMEBOA algorithm based on the transit model by Mandel & Agol (2002) to obtain model parameters; one of which is the mid-transit time. For the transit observed with the T80

telescope on 3 November 2022, it was found to be (in BJD_{TDB}) $T_c = 2459887.4901114$ with a 0.000447 days of uncertainty.

We carefully checked the agreement of the transit depth and duration parameters measured from each light curve that appeared in the literature and paid utmost attention to a consistent analysis with the parameters of the system. As a result, we ensured that all the light curves provide parameters in line with the nature of the system and eliminated those which do not.

3.2 Timing Analysis

After a visual inspection of the TTV diagram, two competing models (see Patra et al. 2017) were fitted to the mid-transit timing data whose mean error is 37.44 ± 15.92 s. The relative qualities of the fits were compared in terms of their χ^2 , AIC and BIC statistics values of fittings. The first model assumes the orbital period to be constant with time:

$$T_{\text{tra}}(E) = T_0 + P \times E \quad (2)$$

where E is the cycle number of orbits with respect to a fixed reference orbit of $T_0(\text{BJD}_{\text{TDB}}) = 2456176.667727068(208)$ (Collins et al. 2017b).

In the second model, we assumed the orbital period to be changing at a constant rate (dP/dE) with time according to the following equation:

$$T_{\text{tra}}(E) = T_0 + P \times E + \frac{1}{2} \frac{dP}{dE} \times E^2 \quad (3)$$

For both models, we sampled the posterior distributions of model parameters with a Markov Chain Monte Carlo (hereafter MCMC) algorithm having 16 chains of 5000 iterations, 500 of which are thrown away as the burn-in period. We made use of the pymc3 code (Allen et al. 2013) for computations of the Gaussian likelihood function and for sampling from the posterior. Median values of the fit parameters are given in Table 2.

As previous transit-timing analyses (Maciejewski et al. 2016; Patra et al. 2017; Maciejewski et al. 2018; Yee et al. 2020; Turner et al. 2021; Wong et al. 2022) suggest, constant period model does not fit WASP-12b transit timings. In contrast, strong evidence for a shrinking orbital period was found in these studies. Our timing model supports this finding with a reduced chi-square $\chi^2_\nu = 9.83$ for the linear model, which is outperformed by the quadratic model with a $\chi^2_\nu = 4.82$. Hence, a significantly better fit to the data than the constant period model was achieved. The superiority of the quadratic fitting can also clearly be seen in Figure 2 which is the TTV diagram based on the corrected linear ephemeris with the parameters in Table 2. In addition to χ^2_ν statistics, Akaike Information Criterion (AIC) and Bayesian Information Criterion (BIC) are widely used in the literature to compare competing models (Schwarz 1978) which are defined with following equations:

$$\text{BIC} = \chi^2 + k \ln n \quad (4)$$

$$\text{AIC} = \chi^2 + 2k \quad (5)$$

where k is the number of free parameters of the fit and n is the number of data points. With $n = 216$ in our TTV diagram, the BIC favors the quadratic model over the linear model by $\Delta\text{BIC} = 1071.545$; as AIC does similarly by $\Delta\text{AIC} = 1074.921$. Although the apsidal precession possibility was not investigated in this study, Patra et al. (2017) states that the

Table 2. Timing Model Fit Parameters. Note that uncertainties in parentheses are the 1σ confidence intervals in the last two digits.

	P (days)	T_0 (BJD _{TDB})	Quadratic term $\frac{1}{2} \frac{dP}{dE}$ (days/orbit)	χ^2_ν	AIC	BIC
Constant Period Model	1.091419027(15)	2456176.667727(21)	-	9.83	2109.404	2116.154
Orbital Decay Model	1.0914202527(39)	2456176.668382(28)	$(-5.364 \pm 0.160) \times 10^{-10}$	4.82	1034.483	1044.609

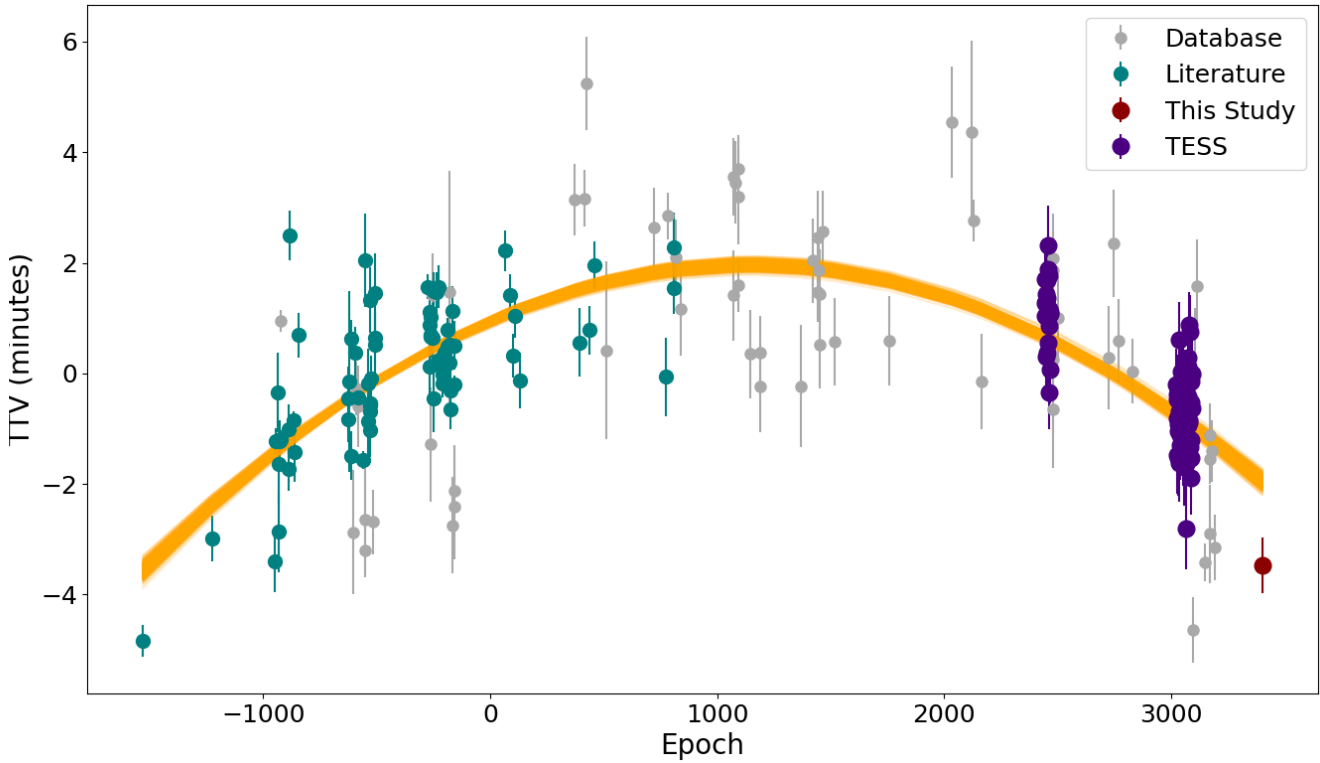


Figure 2. TTV diagram of WASP-12b, after the linear ephemeris is corrected. Yellow parabola indicates the quadratic model with the median values of the posterior distributions of coefficients sampled by the MCMC method, while the shaded region with the same color is limited by the 16th and 84th percentiles of the distributions of quadratic model coefficients.

apsidal precession scenario cannot be completely ruled out, at least further observations are needed to prove it to be invalid, leaving orbital decay scenario as the only option for the evolution of WASP-12 to be investigated with the data at hand. Furthermore, the eccentricity of WASP-12 b's orbit is found to be consistent with zero in many studies, while it was found to be very small in others which decreases possibility of observing an apsidal motion in this system. Only very precise planet occultation observations can confirm both the eccentricity of the orbit if it is non-zero, and the apsidal motion if they are out of phase with transit timings. In the case of an apsidal motion, while the transits are observed earlier than predicted by the linear ephemeris, occultations should be observed later than they are calculated and vice versa. Based on the orbital phase of the occultation mid-point, all occultation observations with Spitzer Space Observatory (Yee et al. 2020; Himes & Harrington 2022) and TESS (Wong et al. 2022) found the eccentricity to be consistent with zero. Follow-up radial velocity studies (Bonomo et al. 2017) found the orbit to be circular as well. Only solution of Husnoo et al. (2012) ($e = 0.018^{+0.024}_{-0.014}$) is slightly out of the 1σ -agreement with a circular orbit. All these findings decrease the potential of apsidal motion to be an explanation for the observed orbital period decline. The

occultation of the planet has a depth of 4800 ppm at the Spitzer $4.5\ \mu\text{m}$ band which can be observed in sufficient precision with the JWST to be able to determine the orbital phase of the secondary and hence the eccentricity of the orbit.

4 Results and Discussion

To generate the TTV diagram for the WASP-12 system, we conducted a homogeneous analysis of the light curves collected over 14 years from both ground-based and space-borne observations.

As Maciejewski et al. (2016) showed, and several other studies (Patra et al. 2017; Maciejewski et al. 2018; Yee et al. 2020; Turner et al. 2021; Wong et al. 2022; Ivshina & Winn 2022) followed, mid-transit times of WASP-12 b were observed earlier than predicted by a linear ephemeris which means that the orbital period has been decreasing since its discovery. Our TTV model supports these findings with a quadratic fit statistically found to be superior to a linear model of the timing data. The first derivative of this model which can be expressed mathematically with a downward parabola, gives the constant rate of the decrease in the orbital period.

Considering the orbital decay model by Eq. 3, the decay rate, expressed in units of days per orbit, is represented by the

variable dP/dE . Based on our analysis, we have calculated a revised period of $P = 1.0914202527 \pm 0.000000039$ days and a decay rate of $dP/dE = -10.73 \pm 0.33 \times 10^{-10}$ days/orbit which is equivalent to $dP/dt = -31.03 \pm 0.94$ ms yr⁻¹. These results correspond to an orbital decay timescale of $\tau = P/|\dot{P}| = 3.04 \pm 0.09$ Myr (see Eq. 5 in [Levrard et al. 2009](#)) between $\tau = 3.25^{+0.24}_{-0.21}$ Myr, ([Yee et al. 2020](#)), and $\tau = 2.90 \pm 0.14$ Myr ([Turner et al. 2021](#)). Moreover, our result for the decay rate agrees with that found by [Wong et al. \(2022\)](#) and [Ivshina & Winn \(2022\)](#) in 1.3σ and 0.7σ , respectively. Both works included the latest TESS sectors in their timing analysis and calculated the decay rate as -29.81 ± 0.94 ms yr⁻¹ and -30.27 ± 1.11 ms yr⁻¹, respectively.

We have already discussed two possible scenarios. However, there might be another reason for such a change. Only a segment of a potentially longer periodic change due to a perturbing body might have been observed so far. Such a change can be modelled with a Keplerian if the additional body is a wide companion inducing a Light-Time Effect (LiTE), or a Newtonian if it is much closer to gravitationally perturb the orbit of WASP-12 b. The latter potential is very low since the tentative linear trend (-4.12 ± 4.37 m s⁻¹ yr⁻¹) in the radial velocities observed by [Bechter et al. \(2014\)](#) helps us to reject the presence of bodies with $m_3 \geq 5 M_{\text{Jup}}$ out to $a_3 \leq 8.3$ au which corresponds to an orbital period of 19.96 years, computed from the Kepler's third law based on the sum of the mass of the host star and the planet adopted from [Chakrabarty & Sengupta \(2019\)](#). This orbital period is only slightly longer than the baseline spanned by the transit timing data. Considering the large amplitude of TTVs (~ 6 minutes), even if the observed change is assumed to be a segment of a variation of a longer periodicity, a very massive body will be needed to induce it which is rejected by the radial velocity observations performed in terms of the "Friends of Hot-Jupiters" survey to look for additional bodies around hot-Jupiter hosting systems ([Bechter et al. 2014](#)).

In the same survey ([Knutson et al. 2014](#)), speckle imaging observations were also performed to look for potential outer companions. [Crossfield et al. \(2012\)](#) and [Bergfors et al. \(2013\)](#) had already detected a visual companion at around $1''$ from WASP-12. [Ngo et al. \(2015\)](#) resolved this companion and found that two nearby sources forming a binary companion (WASP-12 BC) that had been argued to be forming a hierarchical tertiary with WASP-12 based on the preliminary results by [Bechter et al. \(2014\)](#). Based on this assumption, observations of [Bergfors et al. \(2013\)](#) and [Crossfield et al. \(2012\)](#), the images they acquired during their two speckle imaging observation runs separated by 13 months, the system is thought to be composed of a visual binary and WASP-12. Using the magnitude differences between this visual binary and WASP-12 in J, K', K_s bands, [Ngo et al. \(2015\)](#) found the following photometric temperatures for two different observing runs of these two M3 type main sequence stars: 3786 ± 53 K & 3769 ± 44 K for WASP-12 B and 3748 ± 90 K & 3808 ± 49 K for WASP-12 C; and corresponding masses: 0.561 ± 0.022 & $0.554 \pm 0.020 M_{\odot}$ for WASP-12 B and 0.540 ± 0.038 & $0.571 \pm 0.019 M_{\odot}$ for WASP-12 C. They were not able to confirm or rule-out common proper or orbital motion between neither the components of this visual binary nor this pair of stars and WASP-12. They made use of a distance value of 427 ± 90 pc ([Knutson et al. 2014](#)) for the system based on photometric data. This distance from the Gaia-DR3 parallax

is 400 ± 7 pc ([Gaia Collaboration et al. 2016, 2022](#)), hence it is in very good agreement with their finding. However, Gaia cannot resolve the visual pair from WASP-12. On the other hand, according to [Knutson et al. \(2014\)](#), the pair should be separated by 33.68 ± 0.70 au from each other and 426.64 ± 11.63 au from WASP-12 if they are assumed to be at the same distance that Gaia measured. Even if they are gravitationally bound, this binary system cannot induce the observed TTVs during the baseline of observations because they are simply too far away from the planetary system.

Although it cannot be refuted, apsidal motion is unlikely the reason for this secular change either because the eccentricity of the orbit is zero or very low to induce an apsidal motion. It is extremely challenging both to determine the eccentricity precisely and to argue an apsidal motion based on the out-of-phase variations between transit and occultation mid-times because the occultation signal has a very low amplitude. Radial velocities will not be conclusive about the eccentricity either because the precision and frequency of the high resolution spectroscopic observations will not be sufficient unless this target is significantly prioritized by radial velocity programs. Therefore we discarded apsidal motion since it's an unlikely explanation of the observed phenomenon which requires way more precise data to investigate.

Magnetic activity can induce cyclic TTVs too. Spot-induced light curve asymmetries make the measurement of mid-transit times challenging, and hence cause deviations from mid-transit times expected from a linear ephemeris. Based on the visibility, number and total area of stellar spots, the magnitude of these deviations also changes over time and with magnetic activity cycles. In addition, the change in the quadruple moment due to magnetic activity is known to cause variations in the orbital period in turn ([Applegate 1992](#)). However, WASP-12 is a late-F star with a relatively thin convective envelope and is not too young to display strong magnetic activity which has not been reported in its relevant literature either. Moreover, activity-induced TTVs are also cyclic and somewhat chaotic in nature. We haven't observed neither strong in-transit asymmetries nor modulations with stellar rotation in the out-of-transit fluxes attributable to magnetic activity, which haven't been reported in somewhat continuous TESS light curves by other studies either ([Canto Martins et al. 2020](#)). For all these reasons, we assert that the magnetic activity cannot be held responsible either for the large-amplitude TTVs observed in WASP-12 b even if a segment of which is assumed to have been observed so far.

Therefore, we opted to provide an explanation based on tidal interactions between the planet and the star which can also cause an orbital decay. This is a far more likely scenario which is not just the leading but the only mechanism that has been employed to explain the orbital period behaviour of WASP-12 b in its literature. Since the system is not particularly old with $2.0^{+0.7}_{-2.0}$ Gyr age ([Bonomo et al. 2017](#)), the planet is known to have an orbital period shorter than the stellar rotation period, and hence the system is not synchronized yet. Strong tidal interactions between a planet larger than Jupiter on a 1.09 day-orbit and a star larger than our Sun will be very effective in orbital shrinkage ([Ogilvie 2014](#)). The energy transferred to the host stars during these interactions is known to increase the stellar rotation rate. In general, hot Jupiter host stars are found to be rotating faster compared to other planet hosts ([Tejada Arevalo et al. 2021](#)) which can be due to this momentum

Table 3. Orbital Decay analysis results for WASP-12. Source column contains the following sorted by date: 1: Maciejewski et al. (2016), 2: Patra et al. (2017), 3: Maciejewski et al. (2018), 4: Öztürk & Erdem (2019), 5: Yee et al. (2020), 6: Turner et al. (2021), 7: Wong et al. (2022)

$\frac{dP}{dE}$ (days/epoch)($\times 10^{-10}$)	$\frac{dP}{dt}$ (ms yr $^{-1}$)	Q'_* ($\times 10^5$)	τ (Myr)	Source
-8.9 ± 1.4	-25.6 ± 4.0	≈ 2.5	1	1
-10.2 ± 1.1	-29 ± 3	≈ 2.5	3.2	2
-9.67 ± 0.73		1.82 ± 0.32		3
-8.62 ± 0.79		1.76 ± 0.16		4
-10.04 ± 0.69		1.8	$3.25^{+0.24}_{-0.21}$	5
-9.45 ± 0.47	-32.53 ± 1.62	1.39 ± 0.15	2.90 ± 0.14	6
-10.31 ± 0.33	-29.81 ± 0.94	1.50 ± 0.11	3.16 ± 0.10	7
-10.73 ± 0.33	-31.03 ± 0.94	1.72 ± 0.39	3.04 ± 0.09	This work

transfer. A fraction of this energy can also be deposited in the star's envelope. Cold stars with thick convective envelopes are especially effective in depositing this energy; the ratio of which stored in the tidal distortion to the energy dissipated in one orbit of the planet is defined as the tidal quality factor (Q'_*) (Goldreich 1963).

If we assume that the planet's mass stays constant then we can link the rate of change in the orbital period of WASP-12 b to the modified tidal quality factor of its host star by the constant phase lag model of Goldreich & Soter (1966) defined as

$$Q'_* = -\frac{27\pi}{2} \left(\frac{M_p}{M_*}\right) \left(\frac{R_*}{a}\right)^5 \dot{P} \quad (6)$$

where M_p is the mass of the planet, M_* is the mass, R_* is the radius of the host star and a is the semi-major axis of the planet's orbit.

In our calculations, \dot{P} is derived from our timing analysis and the planetary and stellar parameters are used from the references listed in Table 1. Stellar parameters used in this study are in good agreement with the empirical measurements of Stassun et al. (2017). This results in a stellar tidal quality factor of $Q'_* = (1.72 \pm 0.39) \times 10^5$. We provide a list of calculated tidal quality factors for WASP-12 in Table 3. Our result corresponds to the lower bound of the previous values reported for binary star systems between $10^5 - 10^7$ (Meibom et al. 2015; Ogilvie & Lin 2007; Lanza et al. 2011) and for hot Jupiters between $10^5 - 10^{6.5}$ (Jackson et al. 2008; Husnoo et al. 2012; Barker 2020). On the other hand, Hamer & Schlaufman (2019) emphasizes the tendency of host stars of hot-Jupiters to be young, moving towards their host-stars during main-sequence phases of host-star's stellar evolution which requires $Q'_* \leq 10^7$.

The reason for finding lower values of $Q'_* \sim 10^5 - 10^6$ than the theoretical expectations ($10^7 - 10^{10}$; Ogilvie (2014) and references therein) is still unclear. Weinberg et al. (2017) suggested that WASP-12, being a sub-giant star, could be experiencing a more accelerated tidal dissipation as a result of the rupture of internal gravity waves occurring near the core of the star. Furthermore, Barker (2020) computed the rates of tidal dissipation for WASP-12 and showed that the decay rates obtained from theory and observations could only be reconciled if the star was a sub-giant rather than a main-sequence star. In contrast, Bailey & Goodman (2019) investigated this likelihood and found that the identified characteristics of WASP-12 are better suited to the characteristics expected from a main-sequence star as opposed to a sub-giant. However, Gaia photometry (Gaia Collaboration et al. 2016, 2022) finds $\log g = 3.95^{+0.03}_{-0.09}$ which contradicts this argument. Future

studies for the characterization of the host star, especially based on high-resolution spectroscopy and precise-transit photometry, may shed more light on the evolutionary status of WASP-12. A hint gathered from recent infrared observations of a planet's destruction by its potentially sub-giant host (ZTF SLRN-2020, De et al. 2023) could be interpreted as another indicator of the importance of the stellar evolutionary stage in tidal interactions with the planet. The host star of the other very strong candidate system (KOI-4) for orbital decay with convincing observations (Vissapragada et al. 2022) is also a sub-giant star.

Up to the present, WASP-12 b is the only planet whose orbital decay behavior has been convincingly suggested by long-term TTV analysis. However, WASP-12 b probably isn't the only planet we have in this context. WASP-4, KOI-4, WASP-43 and HAT-P-23 are among the possible candidates due to two facts; firstly, their proximity to the host star resulting in a short-period orbit, secondly, large mass leading to strong tidal interactions between the host star and the planet (Rosário et al. 2022; Patra et al. 2020; Harre et al. 2023).

In order to understand the nature and potential reason of the change in the period, more and higher precision observations, especially that of the occultation, are needed. More importantly, there is a strong need for more theoretical advancements in the understanding of tidal interactions between close-in giant planets and their host stars; especially, their ability to dissipate the resultant tidal energy.

5 Summary

Within this study, we provided a new transit observation of WASP-12 b with an 80 cm telescope at AUKR, and measured the mid-transit times from the light curves made available through literature, open databases and telescope archives, forming a TTV diagram with a baseline of nearly 15 years of observations. We compared the linear and quadratic models and found that the latter is a better fit to the TTV data implying an orbital period decay. Using this model we updated the orbital period of WASP-12 b to a new value of $P = 1.0914202527 \pm 0.000000039$ days which gives a decay rate of 31.03 ± 0.94 ms yr $^{-1}$. This result corresponds to an orbital decay timescale of 3.04 ± 0.09 Myr which is shorter than the estimated mass-loss timescale of 300 Myr (Turner et al. 2021).

We attributed this secular change to strong tidal interactions with the host star after discussing potential perturber scenarios, apsidal motion and magnetic activity. WASP-12 has a detected visual binary (Crossfield et al. 2012; Bergfors et al. 2013; Bechter et al. 2014; Ngo et al. 2015) which

may have played an important role in the orbital evolution of WASP-12 b if they were physically bound. They might be responsible for the current close-in position of WASP-12 b and the misalignment between axes of its orbit and the rotation of its host star ($\lambda = 59_{-20}^{+15}$ degrees, [Albrecht et al. 2012](#)) through the well-known Kozai-Lidov mechanism ([Lithwick & Naoz 2011](#)). Since this mechanism causes the eccentricity and orbital inclination change due to the gravitational perturbations by a massive companion on a wide orbit it also causes the planet to migrate inwards, towards the more massive body, which is the host star. This type of migration which is known as high-eccentricity migration, is the leading explanation for the short-period orbits of hot Jupiters ([Fabrycky & Tremaine 2007](#); [Verrier & Evans 2009](#); [Naoz et al. 2011](#)). They are theorized to form further away beyond the snow-line. However, this secular orbital behaviour has a much longer time scale in which the system has lived in its distant past, than the orbital decay we have been most probably observing today in WASP-12 b. While this mechanism may have brought the planet to the close vicinity of its star, strong tidal interactions should have taken over and they are bringing the planet to even closer to its host star and eventual disruption by it.

Based on this most likely scenario, we found the reduced tidal quality parameter (Q'_*) to be $(1.72 \pm 0.39) \times 10^5$ which is almost a magnitude lower than the canonical value (10^6). The reason for this deficiency is still unclear, mostly due to the lack of understanding of the dissipation efficiency of the stellar envelope. Therefore, both continued observations of hot Jupiters with orbital decay potential, including WASP-12 b, and theoretical work to better understand the tidal interactions and the momentum transfer are needed.

Acknowledgments

We thank Ankara University (BAP) for the grant through the project 18A0759001 for the use of T80 telescope at Ankara University Kreiken Observatory (AUKR). This work has made use of data from the European Space Agency (ESA) mission *Gaia*, processed by the *Gaia* Data Processing and Analysis Consortium (DPAC). Funding for the DPAC has been provided by national institutions, in particular the institutions participating in the *Gaia* Multilateral Agreement. Some/all of the data presented in this paper were obtained from the Multimission Archive at the Space Telescope Science Institute (MAST). STScI is operated by the Association of Universities for Research in Astronomy, Inc., under NASA contract NAS5-26555. Support for MAST for non-HST data is provided by the NASA Office of Space Science via grant NAG5-7584 and by other grants and contracts. This research has made use of the NASA Exoplanet Archive, which is operated by the California Institute of Technology, under contract with the National Aeronautics and Space Administration under the Exoplanet Exploration Program.

This paper has made use of the data collected by the TESS mission, available in the Mikulski Archive for Space Telescopes (MAST). Funding for the TESS mission is provided by NASA's Science Mission Directorate. We thank the amateur and professional observers who share their observations through ETD, AXA and ExoClock open databases.

References

Albrecht S., et al., 2012, *ApJ*, 757, 18

- Allen A., DuPrie K., Berriman B., Hanisch R. J., Mink J., Teuben P. J., 2013, in Friedel D. N., ed., *Astronomical Society of the Pacific Conference Series Vol. 475, Astronomical Data Analysis Software and Systems XXII*. p. 387 ([arXiv:1212.1916](#)), [doi:10.48550/arXiv.1212.1916](#)
- Applegate J. H., 1992, *ApJ*, 385, 621
- Babcock H. W., 1961, *ApJ*, 133, 572
- Bailey E., Batygin K., 2018, in *AAS/Division for Planetary Sciences Meeting Abstracts #50*. p. 113.10
- Bailey A., Goodman J., 2019, *MNRAS*, 482, 1872
- Barker A. J., 2020, *MNRAS*, 498, 2270
- Barker A. J., Ogilvie G. I., 2009, *MNRAS*, 395, 2268
- Bechter E. B., et al., 2014, *ApJ*, 788, 2
- Bergfors C., et al., 2013, *MNRAS*, 428, 182
- Bonomo A. S., et al., 2017, *A&A*, 602, A107
- Canto Martins B. L., et al., 2020, *ApJS*, 250, 20
- Chakrabarty A., Sengupta S., 2019, *AJ*, 158, 39
- Chambers J., 2007, in *AAS/Division of Dynamical Astronomy Meeting #38*. p. 6.04
- Chan T., Ingemyr M., Winn J. N., Holman M. J., Sanchis-Ojeda R., Esquerdo G., Everett M., 2011, *AJ*, 141, 179
- Collins K. A., Kielkopf J. F., Stassun K. G., Hessman F. V., 2017a, *AJ*, 153, 77
- Collins K. A., Kielkopf J. F., Stassun K. G., 2017b, *AJ*, 153, 78
- Crossfield I. J. M., Barman T., Hansen B. M. S., Tanaka I., Kodama T., 2012, *ApJ*, 760, 140
- D'Angelo G., Durisen R. H., Lissauer J. J., 2010, in Seager S., ed., *Exoplanets*. University of Arizona Press, pp 319–346, [doi:10.48550/arXiv.1006.5486](#)
- De K., et al., 2023, *Nature*, 617, 55
- Eastman J., Gaudi B. S., Agol E., 2013, *PASP*, 125, 83
- Fabrycky D., Tremaine S., 2007, *ApJ*, 669, 1298
- Gaia Collaboration et al., 2016, *A&A*, 595, A1
- Gaia Collaboration et al., 2022, preprint, ([arXiv:2208.00211](#))
- Goldreich P. M., 1963, PhD thesis, Cornell University, New York
- Goldreich P., Soter S., 1966, *Icarus*, 5, 375
- Hagey S. R., Edwards B., Boley A. C., 2022, *AJ*, 164, 220
- Hamer J. H., Schlaufman K. C., 2019, *AJ*, 158, 190
- Harre J. V., et al., 2023, *A&A*, 669, A124
- Hebb L., et al., 2009, *ApJ*, 693, 1920
- Hiltner W. A., 1962, *Astronomical techniques*. Chicago, University Press
- Himes M. D., Harrington J., 2022, *ApJ*, 931, 86
- Honeycutt R. K., 1992, *PASP*, 104, 435
- Husnoo N., Pont F., Mazeh T., Fabrycky D., Hébrard G., Bouchy F., Shporer A., 2012, *MNRAS*, 422, 3151
- Ivshina E., Winn J., 2022, in *Bulletin of the American Astronomical Society*. p. 102.353
- Jackson B., Greenberg R., Barnes R., 2008, *ApJ*, 681, 1631
- Jenkins J. M., et al., 2016, in Chiozzi G., Guzman J. C., eds, *Society of Photo-Optical Instrumentation Engineers (SPIE) Conference Series Vol. 9913, Software and Cyberinfrastructure for Astronomy IV*. p. 99133E, [doi:10.1117/12.2233418](#)
- Knutson H. A., et al., 2014, *ApJ*, 785, 126
- Lanza A. F., Damiani C., Gandolfi D., 2011, *A&A*, 529, A50
- Levrard B., Winisdoerffer C., Chabrier G., 2009, *ApJ*, 692, L9
- Lithwick Y., Naoz S., 2011, *ApJ*, 742, 94
- Llama J., Vidotto A. A., Jardine M., Fares R., 2013, in *European Planetary Science Congress*. pp EPSC2013–272
- Maciejewski G., Errmann R., Raetz S., Seeliger M., Spaleniak I., Neuhäuser R., 2011, *A&A*, 528, A65
- Maciejewski G., et al., 2013, *A&A*, 551, A108
- Maciejewski G., et al., 2016, *A&A*, 588, L6
- Maciejewski G., et al., 2018, *Acta Astron.*, 68, 371
- Mandel K., Agol E., 2002, *ApJ*, 580, L171
- Meibom S., Barnes S. A., Platais I., Gilliland R. L., Latham D. W., Mathieu R. D., 2015, *Nature*, 517, 589

- Naoz S., Farr W. M., Lithwick Y., Rasio F. A., Teysandier J., 2011, *Nature*, 473, 187
- Ngo H., et al., 2015, *ApJ*, 800, 138
- Ogilvie G. I., 2014, *ARA&A*, 52, 171
- Ogilvie G. I., Lin D. N. C., 2007, *ApJ*, 661, 1180
- Öztürk O., Erdem A., 2019, *MNRAS*, 486, 2290
- Patra K. C., Winn J. N., Holman M. J., Yu L., Deming D., Dai F., 2017, *AJ*, 154, 4
- Patra K. C., et al., 2020, *AJ*, 159, 150
- Poddaný S., Brát L., Pejcha O., 2010, *New Astron.*, 15, 297
- Ricker G. R., et al., 2015, *Journal of Astronomical Telescopes, Instruments, and Systems*, 1, 014003
- Rosário N. M., Barros S. C. C., Demangeon O. D. S., Santos N. C., 2022, *A&A*, 668, A114
- Sada P. V., et al., 2012, *PASP*, 124, 212
- Schwarz G., 1978, *Annals of Statistics*, 6, 461, *ADS*
- Skumanich A., 1972, *ApJ*, 171, 565
- Stassun K. G., Collins K. A., Gaudi B. S., 2017, *AJ*, 153, 136
- Stassun K. G., et al., 2019, *AJ*, 158, 138
- Tejada Arevalo R. A., Winn J. N., Anderson K. R., 2021, *ApJ*, 919, 138
- Turner J. D., Ridden-Harper A., Jayawardhana R., 2021, *AJ*, 161, 72
- Verrier P. E., Evans N. W., 2009, *MNRAS*, 394, 1721
- Vissapragada S., et al., 2022, *ApJ*, 941, L31
- Weinberg N. N., Sun M., Arras P., Essick R., 2017, *ApJ*, 849, L11
- Winn J., 2019, in *AAS/Division for Extreme Solar Systems Abstracts*. p. 201.04
- Wong I., Shporer A., Vissapragada S., Greklek-McKeon M., Knutson H. A., Winn J. N., Benneke B., 2022, *AJ*, 163, 175
- Yee S. W., et al., 2020, *ApJ*, 888, L5

Appendix A: DATA AND LIGHT-CURVES

TESS light curves and EXOFAST model fits can be found in Fig. A1. Mid-transit times calculated from TESS data are in Table A3, and those from ETD and literature are in Tables A1 and A2.

Access:

M23-0201: *Turkish J.A&A* — Vol.4, Issue 2.

Figure A1. TESS transit events from Sectors 20, 43, 44 and 45 of WASP-12b. The best-fitting model obtained from the ExoFASTv1 is shown as a solid red line. The residuals (light-curve minus model) are shown below the light curve. The caption is moved to the top of the figure to increase the readability.

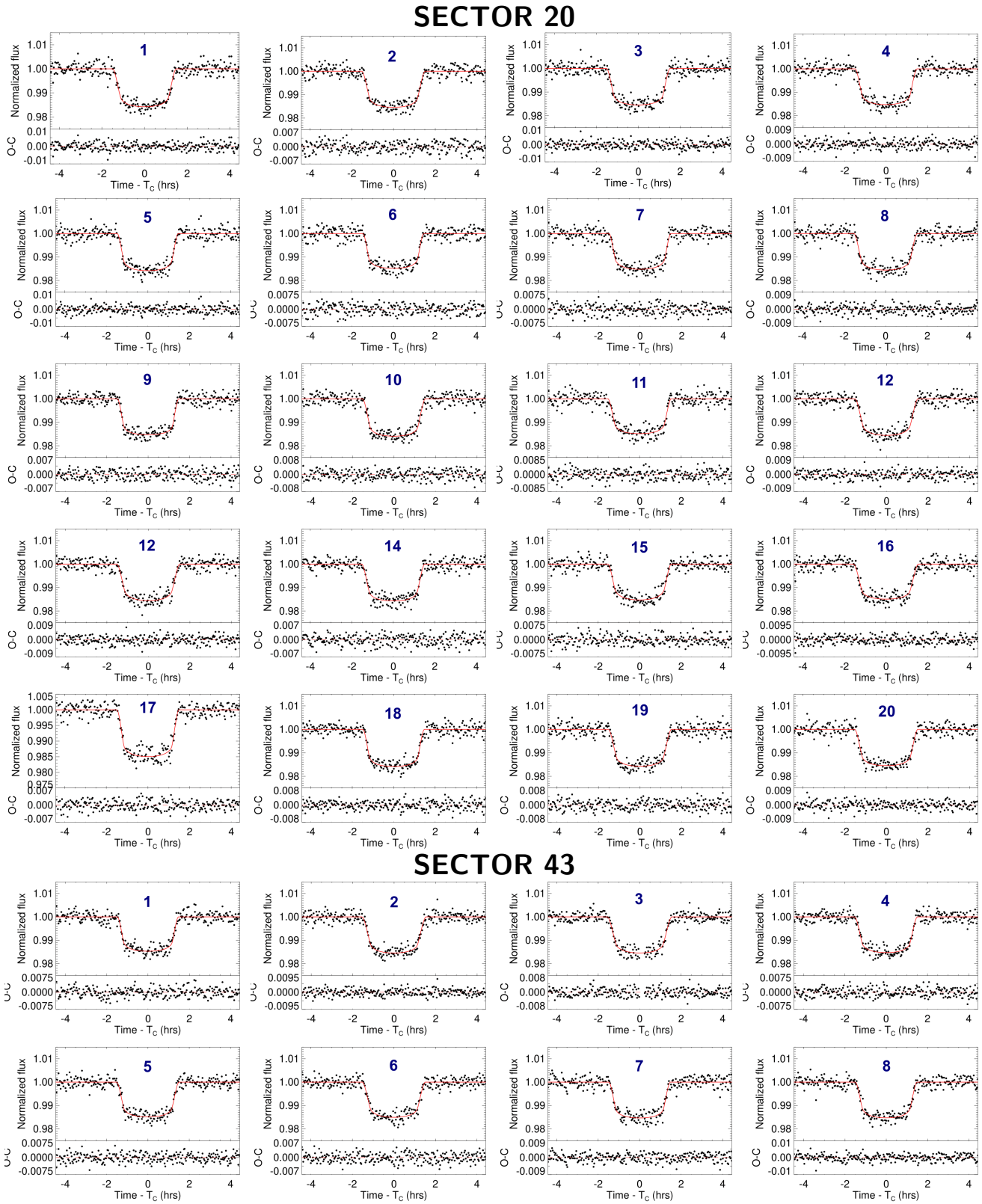
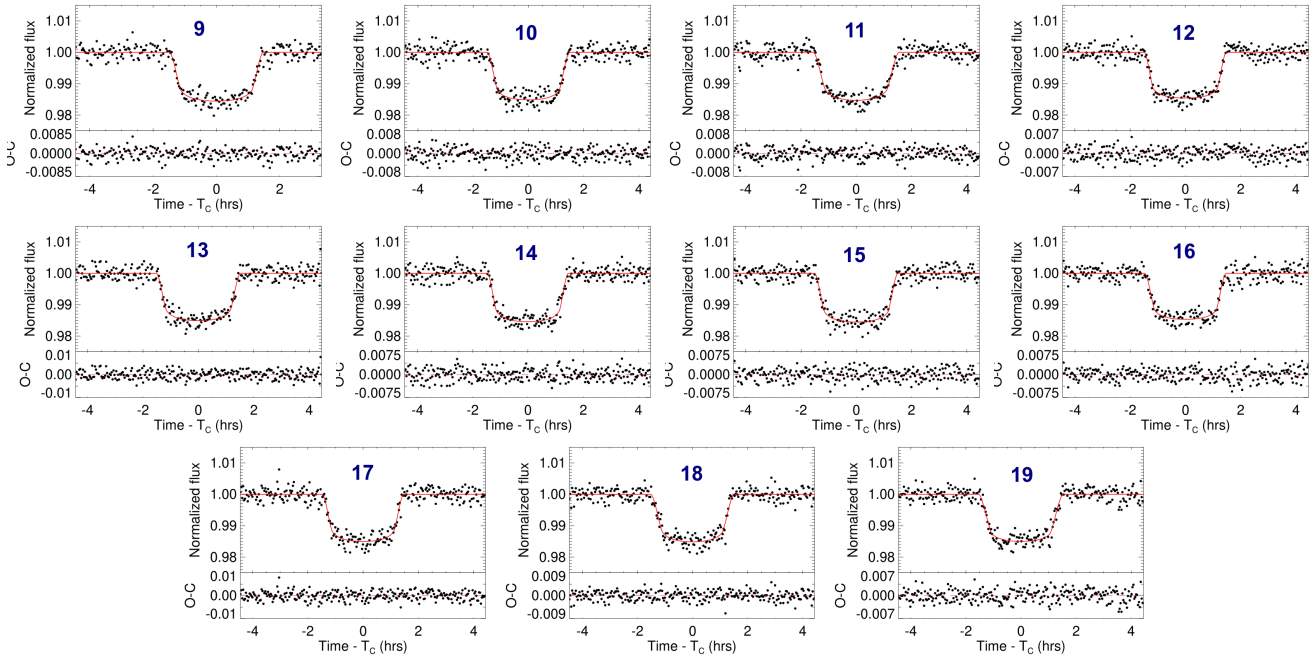


Figure A1 – continued.

SECTOR 43



SECTOR 44

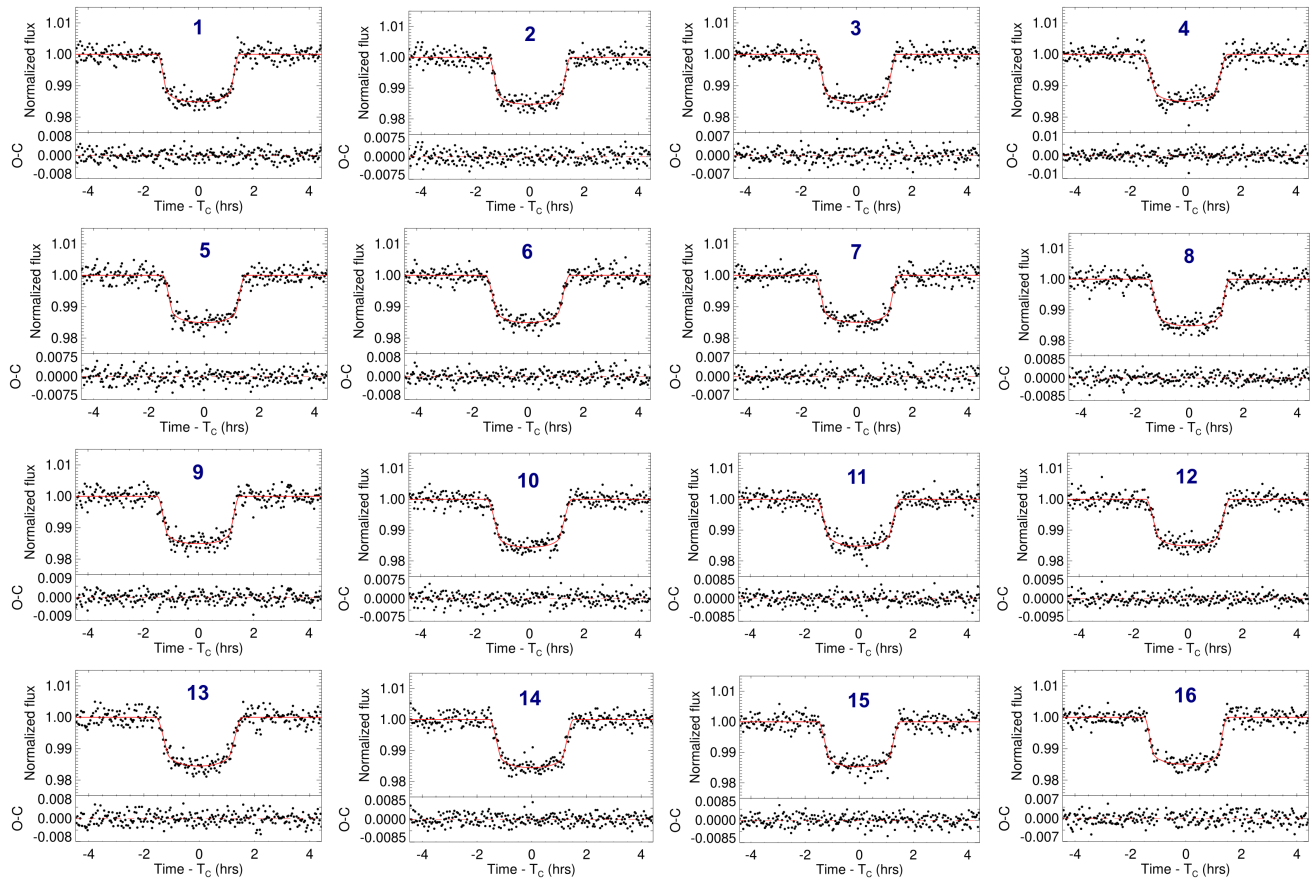
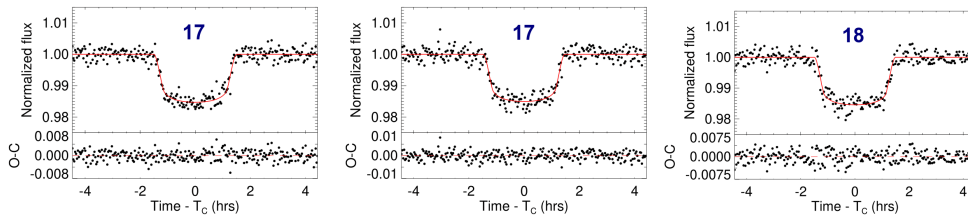


Figure A1 – continued.

SECTOR 44



SECTOR 45

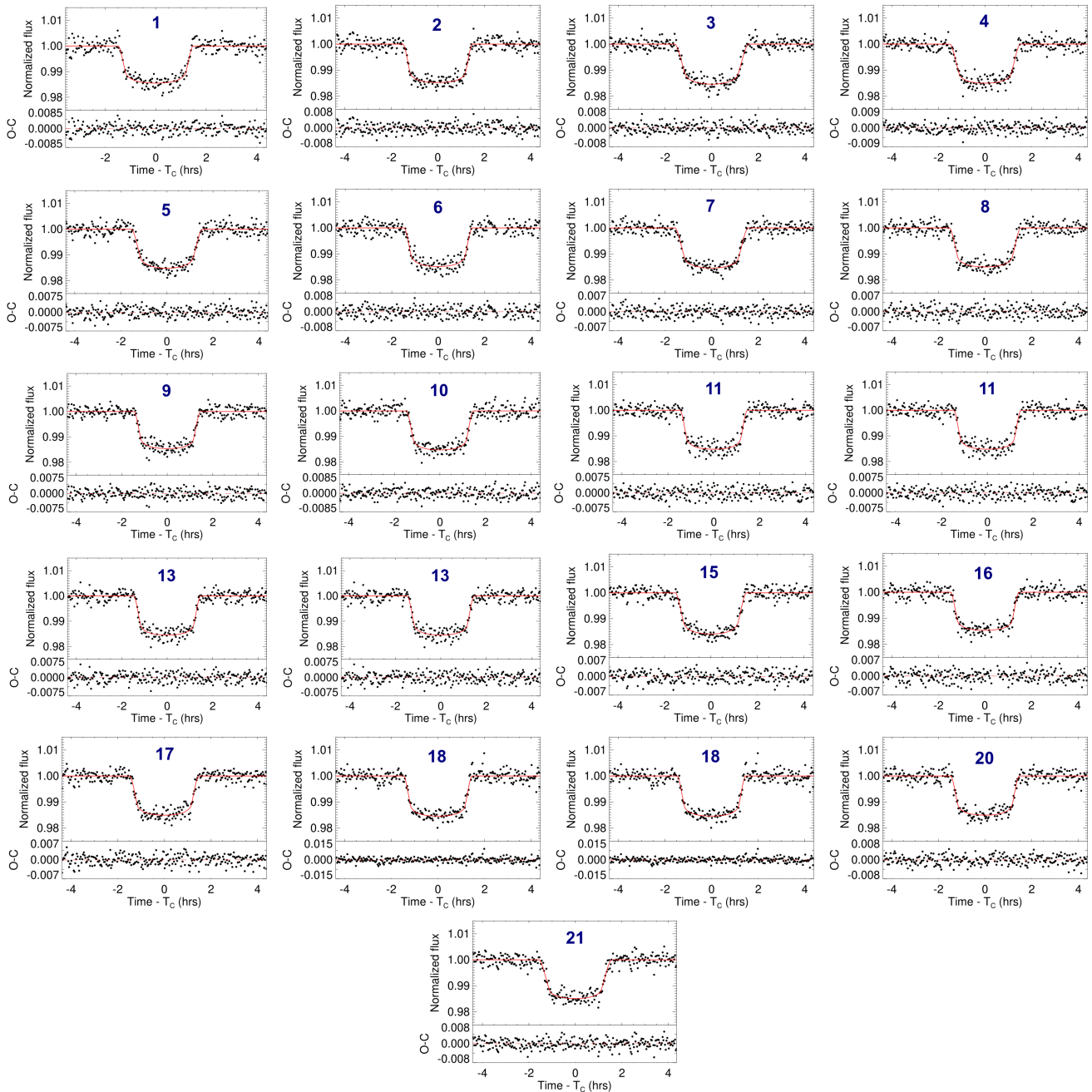


Table A1. Mid-transit times of WASP-12b from Exoplanet Transit Database (ETD). Mid-transit times are in BJD_{TDB} and Error is in days. Source column contains the following observers sorted by their names: 1:Aceti P., 2:Alessandro Marchini, 3:Anael Wunsch, 4:Ayiomamitis A., 5:Benni P., 6:Carreno A., 7:Claudio Arena, 8:David Molina, 9:Dittler U., 10:Rich E. & Irwin S. (Ortega Telescope, Florida Institute of Technology), 11:Enrique Diez Alonso (Instituto Universitario de Ciencias y Tecnologías Espaciales de Asturias (ICTEA) / Departamento de Matemáticas de la Universidad de Oviedo), 12:ESSEIVA Nicolas, 13:Ferran Grau Horta, 14:Francesco Scaggiante & Danilo Zardin, 15:Gaitan J., 16:Garcia R., 17:Ingemyr M. (Nordic Optical Telescope), 18:Irwin S. (Ortega Telescope, Florida Institute of Technology), 19:Ivanov K. (MASTER II, Tunka, Irkutsk State University), 20:Tremosa L., 21:Raetz M., 22:Bretton M., 23:Salisbury M., 24:Bachschmidt M., 25:Naumov K. & Sokov E.N., 26:Naves R., 27:Gomez S.L., 28:Gudmundsson S., 29:Hentunen V.P., 30:Ferrando V., 31:Vrastak M., 32:Kang W., 33:Jongen Y., 34:Zambelli R.

Mid-transit time	Error	Filter	Source	Mid-transit time	Error	Filter	Source	Mid-transit time	Error	Filter	Source
2459526.232430	0.0001347313	V	17	2457069.449942	0.0004777427	Clear	29	2458489.387657	0.0011513425	Clear	28
2455519.631482	0.0007825872	R	26	2457092.369089	0.0005865246	R	23	2458501.392161	0.0002564787	R	22
2455532.730313	0.0003349144	Clear	18	2457344.487060	0.0005656189	Clear	20	2458513.401793	0.0007533295	R	14
2455541.461441	0.0005097237	Clear	34	2457345.579970	0.0004847193	Clear	8	2458537.406967	0.0005938874	R	3
2455577.476462	0.0003352864	Clear	16	2457357.585505	0.0005179041	Clear	8	2458883.388190	0.0004990226	Clear	33
2455577.476853	0.0006697054	R	26	2457357.587790	0.0005279786	Clear	22	2458883.388345	0.0005656367	Clear	3
2455615.676483	0.0004005397	I	10	2457368.499518	0.0006008010	Clear	11	2458884.477868	0.0007422236	I	27
2455889.623632	0.0007197225	Clear	26	2457368.499868	0.0004209166	Clear	22	2458884.478492	0.0009347929	I	27
2455899.448275	0.0005290545	Clear	4	2457369.589827	0.0003409101	Clear	12	2458906.307400	0.0005227777	R	29
2455936.551307	0.0014900924	R	26	2457426.342749	0.000555043	Clear	22	2459147.510503	0.0006495022	R	29
2455982.396164	0.0015234339	V	1	2457474.364772	0.0005624765	Clear	22	2459171.523158	0.0006743217	Clear	30
2455994.398841	0.0006045961	Clear	2	2457474.365203	0.0004601975	Clear	22	2459196.624569	0.0005217855	R	33
2456003.130426	0.0006621090	R	19	2457668.637369	0.0007665793	Clear	8	2459265.383580	0.0004046699	R	13
2456003.130629	0.0005693646	V	19	2457726.484151	0.0005274304	R	31	2459553.514960	0.0004110581	R	28
2456304.368343	0.0005753922	Clear	25	2457750.494975	0.0003675462	Clear	24	2459566.615172	0.0008574575	R	2
2456584.860623	0.0004503138	Clear	5	2457751.587084	0.0005823540	Clear	8	2459576.439075	0.0005781110	R	28
2456630.700239	0.0003558430	Clear	5	2457757.043760	0.0003827669	R	32	2459611.361016	0.0002362983	R	23
2456639.433038	0.0005889406	Clear	9	2457760.317080	0.0005431414	Clear	22	2459635.372586	0.0006219618	R	2
2456722.372800	0.0008129106	R	15	2457761.409142	0.0005568517	Clear	8	2459635.373527	0.0003057812	R	23
2456734.383133	0.0011168902	Clear	6	2457774.506961	0.0005109979	Clear	12	2459636.465251	0.0003895106	R	23
2456734.389285	0.0006271824	V	13	2457832.350777	0.0005458487	Clear	22	2459647.379239	0.0003859405	Clear	21
2456963.582677	0.0005006056	Clear	24	2458096.474198	0.0005617323	Clear	7	2459659.383634	0.0004111139	R	23
2457033.433636	0.0002972191	V	22	2458396.617172	0.0006943350	Clear	33				

Table A2. Mid-transit times of WASP-12b from literature sources. Mid-transit times are in BJD_{TDB} and Error is in days. Source column contains the following articles: 1:Hebb et al. (2009), 2:Chan et al. (2011), 3:Maciejewski et al. (2011), 4:Sada et al. (2012), 5:Collins et al. (2017b)

Mid-transit time	Error	Filter	Source	Mid-transit time	Error	Filter	Source	Mid-transit time	Error	Filter	Source
2454508.976100	0.00020		z	2455903.812656	0.00041878344	R	3	2456006.406709	0.00030541300	R	3
2454840.768775	0.00028818482		i	2455926.733860	0.00026968202	R	3	2455498.896414	0.00113472380	z	4
2455172.561399	0.00012022449	V	2	2455147.458742	0.00016429827	R	3	2455140.908712	0.00038728857	r	5
2455230.406841	0.00012392723	R	3	2455238.046382	0.00037537338	R	3	2455163.830024	0.00025947352	r	5
2455254.419134	0.00027916520	R	3	2455888.533815	0.00014785658	R	3	2455210.761196	0.00031141580	g	5
2455920.185274	0.00025801119	R	3	2455890.716409	0.00012269452	R	3	2455209.669269	0.00027154017	r	5
2455566.563402	0.00011269846	R	3	2455959.475603	0.00009267431	R	3	2455509.809670	0.00030716553	r	5
2455600.398109	0.00013706603	R	3	2455158.373545	0.00049723600	R	3	2455510.902563	0.00023184657	r	5
2455601.489504	0.00015086379	R	3	2455159.463211	0.00051404042	R	3	2455984.577531	0.00025781763	r	5
2455876.528583	0.00015384862	R	3	2455160.555478	0.00049569959	R	3	2455985.669190	0.00030176938	r	5
2455946.378294	0.00018859365	R	3	2455494.530530	0.00039893980	R	3	2455996.584369	0.00031179239	r	5
2455947.469793	0.00016535669	R	3	2455575.297265	0.00058434563	R	3	2456249.794341	0.00025625452	r	5
2455948.561029	0.00017722940	R	3	2455530.547926	0.00032309552	R	3	2456273.805005	0.00025575108	r	5
2455970.389863	0.00012130445	R	3	2455542.552971	0.00012302307	R	3	2456284.718428	0.00027618179	r	5
2455971.481498	0.00015553004	R	3	2455887.442302	0.00013739039	R	3	2456297.815956	0.00026930189	r	5
2455982.395280	0.00014021010	R	3	2455888.533573	0.00022610089	R	3	2456319.643530	0.00034820665	r	5
2455983.486919	0.00014906743	R	3	2455923.458675	0.00009861251	R	3	2456607.778629	0.00042732300	V	5
2455215.129301	0.00030910288	R	3	2456005.314798	0.00012105256	R	3	2457059.627293	0.00044104412	r	5
2455601.489427	0.00033149730	R	3	2455600.398111	0.00038617150	R	3	2457060.718206	0.00032577952	r	5
2455623.318728	0.00032883326	R	3	2455624.410713	0.00050219019	R	3	2455603.672674	0.00028424353	r	5
2455624.410064	0.00042879617	R	3	2455494.530259	0.00028051129	R	3	2455903.814008	0.00023675420	Kepler	5
2455887.442454	0.00029176705	R	3	2455590.575584	0.00043619427	R	3	2456654.709800	0.00030100412	r	5
2455888.533592	0.00028435457	R	3	2455600.397770	0.00034089466	R	3	2456677.630415	0.00029505565	r	5
2455589.483693	0.00051321317	R	3	2455601.490822	0.00041502078	R	3	2457023.608842	0.00049246658	r	5
2455901.630580	0.00043826180	R	3	2455887.441771	0.00033159693	R	3				

Table A3. WASP-12b transit times from TESS. Light-curve numbers (blue colored on Fig. A1) are given in parentheses next to the sector number. Mid-transit time is in BJD_{TDB} and Error is in days.

Sector	Mid-transit time	Error	Sector	Mid-transit time	Error
20(1)	2458844.096692	0.00049540361	43(1)	2459476.027289	0.00044611349
20(2)	2458845.187957	0.00048180112	43(2)	2459477.118514	0.00046182277
20(3)	2458846.279835	0.00048259208	43(3)	2459478.209235	0.00048889969
20(4)	2458847.370981	0.00048426449	43(4)	2459479.301121	0.00043708329
20(5)	2458848.462485	0.00046781794	43(5)	2459480.392833	0.00045585344
20(6)	2458849.553122	0.0004717019	43(6)	2459481.483794	0.00046496648
20(7)	2458850.645223	0.00045744376	43(7)	2459482.574878	0.00048099246
20(8)	2458851.736009	0.00050059869	43(8)	2459483.667157	0.00044333311
20(9)	2458852.828337	0.00041634711	43(9)	2459484.758141	0.00045191458
20(10)	2458853.919533	0.00046562619	43(10)	2459488.033454	0.00047297004
20(11)	2458858.284643	0.00055127472	43(11)	2459489.123334	0.00048805679
20(12)	2458859.377287	0.00050552209	43(12)	2459490.215393	0.00041412175
20(13)	2458860.468404	0.00044858376	43(13)	2459491.306520	0.00045713561
20(14)	2458861.558276	0.00046310746	43(14)	2459492.398435	0.00042565278
20(15)	2458862.650537	0.00048840382	43(15)	2459493.489230	0.00043644263
20(16)	2458863.742166	0.00053756448	43(16)	2459494.581304	0.00046583763
20(17)	2458864.834006	0.00043186085	43(17)	2459495.672643	0.00045984243
20(18)	2458865.924245	0.00042267147	43(18)	2459496.764407	0.00047928386
20(19)	2458867.016356	0.0005088068	43(19)	2459497.855337	0.0004978744
20(20)	2458868.107799	0.00047878919			
44(1)	2459502.220997	0.00041747023	45(1)	2459526.232430	0.00051302815
44(2)	2459503.312851	0.00044850912	45(2)	2459527.323601	0.00044447508
44(3)	2459504.403562	0.00042563671	45(3)	2459528.415230	0.00049101922
44(4)	2459505.494859	0.0005324653	45(4)	2459529.506669	0.00050317911
44(5)	2459506.586329	0.00046807366	45(5)	2459530.598457	0.00049006501
44(6)	2459507.678071	0.00047147983	45(6)	2459531.689992	0.00046251739
44(7)	2459508.769936	0.0004558675	45(7)	2459532.780569	0.00044033805
44(8)	2459509.860678	0.00045340335	45(8)	2459533.872027	0.00045730201
44(9)	2459510.952238	0.00049258687	45(9)	2459534.964662	0.00041824334
44(10)	2459514.225912	0.00048365134	45(10)	2459536.054890	0.00046922117
44(11)	2459515.317421	0.00050257145	45(11)	2459537.146897	0.00043641757
44(12)	2459516.409020	0.00047652264	45(12)	2459540.420320	0.00047940023
44(13)	2459517.501106	0.00053612959	45(13)	2459541.511636	0.00041134368
44(14)	2459518.592534	0.00047356141	45(14)	2459542.604512	0.00045940793
44(15)	2459519.682242	0.00051514981	45(15)	2459543.695047	0.0004330709
44(16)	2459520.775233	0.00043540286	45(16)	2459544.785512	0.00045892702
44(17)	2459521.866261	0.0004320403	45(17)	2459545.877181	0.00043398382
44(18)	2459522.957303	0.00046212504	45(18)	2459546.968826	0.00043300059
44(19)	2459524.049699	0.00042685725	45(19)	2459548.060986	0.00051846544
			45(20)	2459549.152063	0.00042613561
			45(21)	2459550.243920	0.000526486